JPSA
Japan Poultry Science Association

http://www.jstage.jst.go.jp/browse/jpsa
doi:10.2141/jpsa.2025002
Copyright © 2025, Japan Poultry Science Association.

Network Pharmacology Suggests Mechanisms for Therapeutic Effects of *Caulis Sinomenii* on Avian Gout

Guanyang Li [1, 2 †], Junfei Xu [2 †], Huanhuan Li [2], Wenxin Yan [2], Fengting Chen [2], Anwen Yuan [1] and Juzuo Zhang [1, 2]

[1] Department of Clinic Veterinary Medicine, College of Veterinary Medicine, Hunan Agricultural University, Changsha 410128, China.
[2] College of Biological and Food Engineering/Key Laboratory of Research and Utilization of Ethnomedicinal Plant Resources of Hunan Province/Hunan Provincial Higher Education Key Laboratory of Intensive Processing Research on Mountain Ecological Food, Huaihua University, Huaihua 418000, China.

Avian gout (AG) is detrimental to the survival and production performance of poultry and effective drugs are lacking. *Caulis sinomenii* has shown clinical efficacy against arthritis and may have potential value in AG prevention and treatment. In the present study, the components and targets of *C. sinomenii* and AG-related targets were identified using relevant databases. The common targets, target interactions, and signaling pathways involved in the prevention and treatment of AG by *C. sinomenii* were determined using software to explore the potential mechanisms of action. Sixteen components of *C. sinomenii*, eight of which were active ingredients with 351 targets and 2993 AG-related targets, were identified using several databases. A total of 156 common targets were associated with 202 biological processes and 34 pathways. Toll-like receptor 4 (TLR4) and prostaglandin endoperoxide synthase 2 were core targets. These targets may exert therapeutic effects on AG through four pathways: the nucleotide-binding oligomerization domain (NOD)-like receptor, mammalian target of rapamycin, TLR, and mitogen-activated protein kinase signaling pathways. In summary, *C. sinomenii* has potential therapeutic efficacy against AG through multicomponent, multi-target, and multi-pathway mechanisms.

Key words: avian gout, *Caulis sinomenii*, molecular docking, network pharmacology

J. Poult. Sci., 62: jpsa.2025002, 2025

Introduction

With the development of modern animal husbandry, most breeders use intensive breeding methods and high-calcium and high-protein feed to increase egg production and growth rate of poultry, further exacerbating the incidence of avian gout (AG). According to statistics, chickens between 20 and 50 days of age and those over 80 days of age are more susceptible to AG, which is a common disease in the poultry industry[1,2]. AG pathogenic factors include genetics, nutrition, infectious diseases, feeding management, and poisoning, which lead to high uric acid content in the blood, eventually leading to the accumulation of urate crystals in the joints and internal organs[3]. Recently, astrovirus has been identified as the main pathogen that causes AG. Astroviral infection, associated with visceral gout and kidney disease, has a morbidity rate of up to 80% and a mortality rate of up to 50% in poultry with AG[1,2,4–6], causing severe economic losses.

Clinically, AG is divided into visceral and joint gout. Visceral gout is a common metabolic disease characterized by high uric acid levels in the blood, which lead to urate deposition on the surfaces of internal organs[7]. Joint gout has typical clinical symptoms of limited movement, obvious swelling of the legs and wings, loss of appetite, listlessness, and white watery stools. Additionally, its pathological changes in sick chickens mainly manifest as white urate crystal deposition in swollen joints, viscera, renal tubules, and ureters[8]. These symptoms severely affect the health and survival of poultry, reducing their quality of life. Moreover, AG strongly affects egg production, growth velocity, and the reproductive ability of poultry, causing great harm to the poultry industry and the birds themselves.

Received: October 21, 2024, Accepted: December 4, 2024
Available online: January 8, 2025
Correspondence: Anwen Yuan (yuananweny@163.com) or Juzuo Zhang (juzuo_zhang@163.com), College of Biological and Food Engineering, Huaihua University; No. 180 Huaidong Road, Hecheng District, Huaihua, 418000, China.
† These authors contributed equally to this study.
The Journal of Poultry Science is an Open Access journal distributed under the Creative Commons Attribution-NonCommercial-ShareAlike 4.0 International License. To view the details of this license, please visit (https://creativecommons.org/licenses/by-nc-sa/4.0/).

Currently, colchicine, nonsteroidal medicines, and glucocorticoid drugs are used to effectively treat AG by eliminating joint inflammation[9]. Moreover, bupivacaine, polyparabanic acid uricase, and methionine hydroxy analogs are effective in treating AG because these drugs acidify and remove excess uric acid from urine and promote the excretion of excess calcium from the body[10,11]. Additionally, allopurinol effectively treats AG by inhibiting uric acid synthesis[12,13]. However, the side effects of these drugs severely hinder the practical application, which in turn reduces the effect on production performance. Thus, new anti-AG drugs are urgently required.

C. sinomenii, also known as Fenglong, is a traditional Chinese herbal medicine that contains alkaloids, volatile oils, lipids, sterols, triterpenes, and other chemical components[14]. It has analgesic, anti-inflammatory, immunosuppressive, and anti-arthritic properties[15], and its roots and stems have long been used to treat rheumatoid arthritis in southern China[16]. However, the specific mechanism of action remains unclear. In the present study, network pharmacology and molecular docking analyses were used to explore the therapeutic effects of *C. sinomenii* in the treatment of AG. Using a literature search and network pharmacology analysis, the active components of *C. sinomenii* and the potential disease-related targets and pathways involved in the treatment of AG by *C. sinomenii* were predicted. Molecular docking simulation validation was performed for the main active components and core proteins to explore the mechanism of action of *C. sinomenii* during AG treatment.

Materials and Methods

Screening of drug- and disease-related targets and identification of common targets

First, the Traditional Chinese Medicine Systems Pharmacology Database and Analysis Platform (TCMSP) (https://old.tcmspe.com/tcmsp.php/) was used to search the chemical names of the active ingredients to obtain the corresponding PubChem CId numbers. The active ingredients with an oral bioavailability (OB) ≥ 30% and a drug likeness index (DL) ≥ 0.18 were identified[17,18]. Active ingredients that did not meet the screening criteria, but were still used to treat gout were also identified using the literature[19–22]. Key targets of the active ingredients of *C. sinomenii* were identified using PubChem (https://pubchem.ncbi.nlm.nih.gov/) to obtain the corresponding canonical Simplified Molecular Input Line Entry System (SMILES) data and targets with probabilities greater than 0 were selected using the Swiss Target Prediction database (http://www.swisstargetprediction.ch/)[23]. Second, the keywords "gout," "gout arthritis," "avian gout," "hyperuricemia," and "*Mycoplasma synoviae* infection" were used to search the GeneCards (https://www.genecards.org/), Online Mendelian Inheritance in Man (OMIM) (http://www.omim.org/), and the Therapeutic Target Databases (TTD) (https://db.idrblab.net/ttd/) to obtain AG-related targets[24,25]. Finally, the targets obtained in the aforementioned two steps were imported into Venny 2.1.1 (https://bioinfogp.cnb.csic.es/tools/venny/index.html) to identify the potential AG-related targets of *C. sinomenii*[26].

The common targets were imported into Cytoscape 3.10.2 software to construct a "drug-ingredient-disease-target" network diagram. This was followed by further analysis of the common targets to determine the interactions between the active components and disease-related targets.

Construction of the protein–protein interaction (PPI) network

Common targets were imported into the "multiple proteins" module of the Search Tool for the Retrieval of Interacting Genes/Proteins (STRING) database (http://string-db.org/)[27], with the minimum value of interaction set to 0.4; the species was set to *Gallus gallus* to obtain the tab-separated values file of the PPI network. A protein interaction map was constructed using Cytoscape version 3.10.2.

To accurately analyze the biological processes and signaling pathways associated with the prevention and treatment of AG by *C. sinomenii*, Gene Ontology (GO) and Kyoto Encyclopedia of Genes and Genomes (KEGG) pathway enrichment analyses of key targets were conducted. Common targets were imported into the Database for Annotation, Visualization, and Integrated Discovery (DAVID) web tool (http://david.ncifcrf.gov/) with the species set as *Gallus gallus*. The top 10 enriched biological process (BP), cellular component (CC), and molecular function (MF) terms in the GO analysis and the enriched pathways in the KEGG pathway analysis were identified using $P < 0.01$ as the screening criterion. Enriched terms were then visualized as bubble plots and charts using the SRplot platform (https://www.bioinformatics.com.cn/).

Molecular docking

Based on the literature, eight core targets were selected as receptors, and eight active components identified in *C. sinomenii* were used as ligands for molecular docking validation. First, the three dimensional (3D) structures of the eight active components of *C. sinomenii* were downloaded from PubChem. The 3D structure was hydrogenated and exported as a pdbqt file using the AutoDock Tools software and the core target protein files were downloaded from the UniProt database (https://www.uniprot.org/). In the absence of 3D structural data for the targets, the amino acid sequences were imported into Swiss-Model (https://swissmodel.expasy.org/) for prediction purposes. The results with the highest prediction scores were selected. Following the removal of water molecules, solvent molecules, and ions from the target protein structure using the Python molecule (PyMOL) software, hydrogenated pdbqt files were obtained using the AutoDock Tools software. Finally, the resulting small and large receptor molecules were imported into AutoDock Tools to calculate the corresponding binding energies.

PyMOL software was used to construct a schematic diagram of the key active components and core target proteins of *C. sinomenii*, and the molecular docking of the key active components and core target proteins was visualized[28].

Molecular dynamics (MD) simulation

MD simulations were performed using the Gromacs 2022.1 program[29] with the Amber14sb force field under constant tem-

perature, pressure, and periodic boundary conditions. Molecules were placed in a cubic box of 8.0 nm × 8.0 nm × 8.0 nm, and Amber14sb was used in all simulations. For the all-atom force field, the transferable intermolecular potential 3 points water model[30] was used to solvate protein and small-molecule complexes. The initial structure was subjected to energy minimization for 50,000 steps using the steepest descent method. The isothermal-isobaric ensemble was used in the simulations and the operational equations were integrated using the Leap-Frog method. The properties-method-event method[31] was used for long-range electrostatic interactions. The cut-off distance of the van der Waals and Coulomb interactions was 12 Å, and updates were performed every 10 steps. The Lincs algorithm[32] was used to constrain all bond lengths with the parameters lincs_iter = 1 and lincs_order. = 4. The system temperature was increased from 0 K to 298.15 K via a V-rescale temperature coupler[33]. The Parrinello—Rahman method[34] was used to control the system at a constant pressure of 1 bar and maintain pressure isotropy. Mesh denoising via a neighborhood scheme was used to calculate non-bonded interactions, with short and long cut-off distances of 9 Å and 14 Å, respectively. The criteria for hydrogen bond formation were that the donor–acceptor angle was less than 30° and that the donor–acceptor interatomic distance was less than 0.35 nm. The initial velocities were randomly assigned using the Maxwell—Boltzmann distribution. A total of 50,000,000 simulation steps were performed, the time step size was 2 fs, the total simulation time was 100 ns, and 10,000 conformations were generated. The simulation results were visualized using the Gromacs embedded program and Visual Molecular Dynamics software.

Molecular toxicity prediction

Molecular toxicity was predicted according to previously described methods[35]. Molecular structures of the active ingredients were obtained from PubChem (https://pubchem.ncbi.nlm.nih.gov/). The SMILES numbers or molecular structures of the active ingredients were imported into the ProTox database (https://tox.charite.de/) to predict the molecular toxicity. Toxic doses were expressed as lethal dose 50 (LD50) values (mg/kg body weight). Toxicity classes were defined according to the globally harmonized system of classification of chemical labeling (GHS). LD50 values are given in [mg/kg]: class I is fatal if swallowed (LD50 ≤ 5); class II is fatal if swallowed (5 < LD50 ≤ 50); class III is toxic if swallowed (50 < LD50 ≤ 300); class IV is harmful if swallowed (300 < LD50 ≤ 2000); class V is possibly harmful if swallowed (2000 < LD50 ≤ 5000); and class VI was nontoxic (LD50 > 5000).

Results

Eight active components and 351 targets may play a role in C. sinomenii treatment of AG

In the TCMSP database, eight effective active ingredients, including higenamine (MOL002419) (Figure 1A), β-sitosterol (MOL000358) (Figure 1B), michelenolide (MOL000623) (Figure 1C), sinomenine (MOL000625) (Figure 1D), magnograndiolide (MOL000622) (Figure 1E), stepholidine (MOL000627) (Figure 1F), 16-epi-isositsirikine (MOL000621) (Figure 1G), and magnoflorine (MOL000764) (Figure 1H), were identified as meeting the screening criteria or have been used in AG prevention and treatment. Alkaloids present in *C. sinomenii*, such as sinomenine, have been demonstrated to exhibit favorable therapeutic effects for the treatment of rheumatic paralysis and joint swelling. Terpene lactones have anti-inflammatory and analgesic effects and are, therefore, typically employed in the treatment of inflammatory conditions, such as rheumatoid arthritis. Higenamine has anti-inflammatory effects on lipopolysaccharide (LPS)-induced mouse microglia (BV2 cells) through the regulation of the nuclear factor-κB (NF-κB) and nuclear factor erythroid 2-related factor 2/heme oxygenase-1 (Nrf2/HO-1) signaling pathways, where the regulation of the HO-1 and phosphoinositide 3-kinase/Akt/Nrf-2 (PI3K/Akt/Nrf-2) signaling pathways alleviate collagen-induced arthritis[19,22]. Moreover, magnoflorine inhibits inflammation by regulating the NF-κB, mitogen-activated protein kinase (MAPK), and PI3K/Akt signaling pathways, delaying cartilage degradation and preventing the exacerbation of osteoarthritis[21]. After prediction using the Swiss Target Prediction database, and merger and deduplication, 351 component targets of *C. sinomenii* were ultimately predicted (Figure 1I).

C. sinomenii may treat AG through multiple targets

The relevant target genes of AG were identified using the GeneCards, OMIM, and TTD databases, and literature; a total of 2993 target genes were obtained. After comparing the 2993 AG-related targets and the 351 targets of the *C. sinomenii* active components, a total of 156 key targets were identified (Figure 1I). These common targets represent those through which *C. sinomenii* exerts its therapeutic effects on AG. To understand the relationships between the active ingredients from *C. sinomenii* and these targets, a network diagram of "*C. sinomenii*-active ingredient-target-AG" was constructed (Figure 1J). The image shows eight active ingredients that interact with potential targets. There are 157 nodes and 389 edges. The dark green ellipses in the figure represent common targets, the light green rectangles represent the effective active ingredients of the drug, the red hexagons at the top represent drugs, and the red triangles below represent diseases. Each edge represents the interaction between *C. sinomenii* and the active ingredient, active ingredient and target, or target and disease.

Signal transducer and activator of transcription 3 (STAT3), nonreceptor tyrosine kinase (SRC), matrix metalloproteinase 9 (MMP9), hypoxia-inducible factor 1A (HIF1A), peroxisome proliferator activated receptor G (PPARG), Toll-like receptor 4 (TLR4), transcription factor AP-1 (JUN), prostaglandin endoperoxide synthase 2 (PTGS2), and inducible nitric oxide synthase 2 (NOS2) might be core targets of C. sinomenii in the treatment of AG

The PPI network diagram further demonstrated the interactions between common targets. Each node represents a protein and each edge represents a different interaction. The PPI network graph contained 130 nodes and 520 edges (Figure 2A). Samples were imported into Cytoscape 3.10.2 software for PPI visualiza-

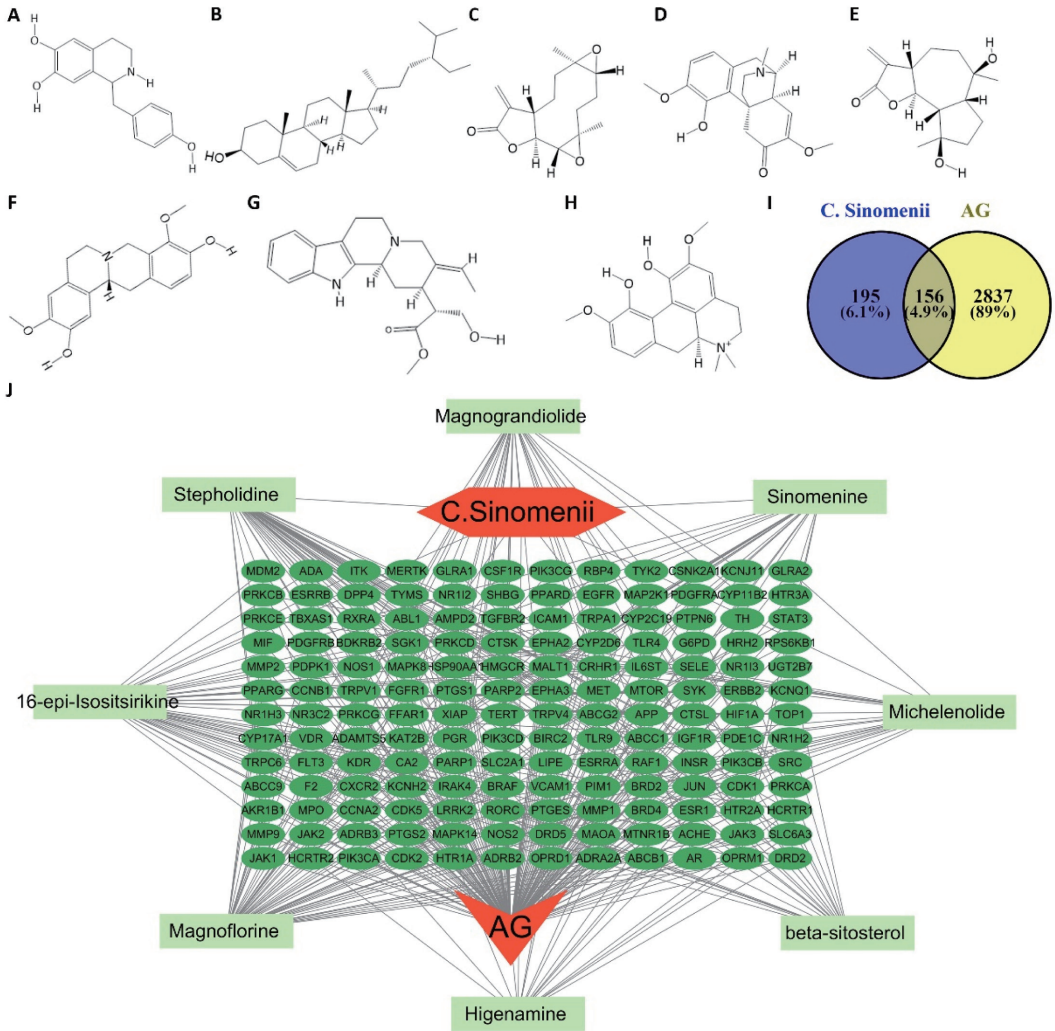

Fig. 1. **The active components of *C. sinomenii* and the "*C. sinomenii*-active ingredient-target-avian gout (AG)" network diagram.**

(A) Two dimensional (2D) structure diagram of higenamine. (B) 2D structure diagram of β-sitosterol. (C) 2D structure diagram of michelenolide. (D) 2D structure diagram of sinomenine. (E) 2D structure diagram of magnograndiolide. (F) 2D structure diagram of stepholidine. (G) 2D structure diagram of 16-epi-Isositsirikine. (H) 2D structure diagram of magnoflorine. (I) Venn diagram of *C. sinomenii* and AG-related targets. (J) Network diagram of "*C. sinomenii*--active ingredients-common targets–AG".

tion. The larger the degree value, the darker the color and the larger the circle. Moreover, software analysis revealed that the average degree value was 8, and 42 target points were greater than the average value. According to the literature and degree ranking, STAT3 (AF_AFQ6DV79F1: https://www.uniprot.org/structure/af_afq6dv79f1), SRC (AF_AFP00523F1: https://www.uniprot.org/structure/AF_AFP00523F1), MMP9 (Swiss-Model forecasting), HIF1A (AF_AFQ9YIB9F1: https://www.uniprot.org/structure/AF_AFQ9YIB9F1), PPARG (AF_AFA0A3Q2U209F1: https://www.uniprot.org/structure/AF_AFA0A3Q2U209F1), TLR4 (AF_AFC4PCF3F1: https://www.uniprot.org/structure/AF_AFC4PCF3F1), JUN (AF_AFP18870F1: https://www.uniprot.org/structure/AF_AFP18870F1), PTGS2 (AF_AFP27607F1: https://www.uniprot.org/structure/AF_ AFP27607F1), and NOS2 (AF_AFQ90703F1: https://www.uniprot.org/structure/AF_AFQ90703F1) might be key targets that play important regulatory roles in the treatment of AG (Figure 2B).

C. sinomenii played important roles in AG by regulating the NOD-like receptor pathway and the mammalian target of rapamycin (mTOR), TLR, and MAPK signaling pathways

GO functional and KEGG pathway enrichment analyses were performed on 156 common targets using the DAVID web tool (*P*

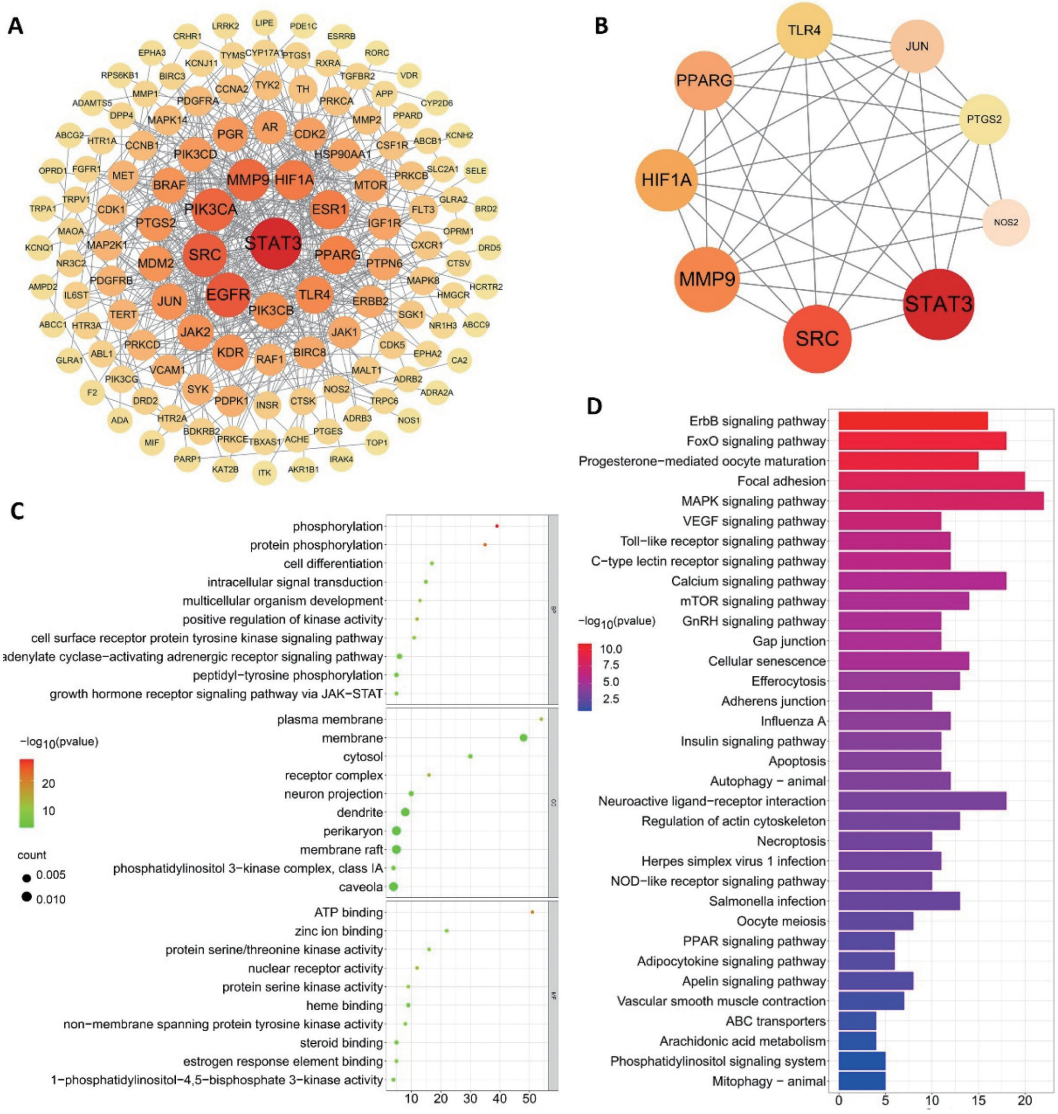

Fig. 2. **Network pharmacology prediction of the mechanism by which *C. sinomenii* treats avian gout (AG).** (A) Map of the potential targets in the protein-protein interaction (PPI) network that are involved in the treatment of AG by *C. sinomenii*. (B) Map of the core targets in the PPI network that are involved in the treatment of AG by *C. sinomenii*. (C) Graph of the gene ontology (GO) enrichment analysis results. (D) List of the enriched Kyoto Encyclopedia of Genes and Genomes (KEGG) pathways. Signal transducer and activator of transcription 3 (STAT3); nonreceptor tyrosine kinase (SRC); matrix metalloproteinase 9 (MMP9); hypoxia-inducible factor 1A (HIF1A); peroxisome proliferator activated receptor G (PPARG); Toll-like receptor 4 (TLR4); transcription factor AP-1 (JUN); prostaglandin endoperoxide synthase 2 (PTGS2); inducible nitric oxide synthase 2 (NOS2).

<0.01) (Figure 2C and D). GO analyses revealed 202 enriched terms, including 119 BP terms that were involved in protein phosphorylation, positive regulation of kinase activity, and the cell surface receptor protein tyrosine kinase signaling pathway. Additionally, 26 CC terms were enriched, including receptor complex, plasma membrane, and phosphatidylinositol 3-kinase complex, whereas 57 MF terms were enriched, including ATP binding, nuclear receptor activity, and protein serine kinase activity. The enriched terms were arranged in ascending order according to the *P* value. The top 10 BP, CC, and MF terms are displayed in the bubble chart, where the horizontal axis represents the value and the vertical axis represents the gene name. The intensity of the colors indicates a high degree of confidence. These results suggested that *C. sinomenii* might be used to treat

AG through the regulation of various BPs. In the KEGG pathway enrichment analysis, 156 common targets were enriched in 34 pathways, and the main pathways involved the NOD-like receptor, mTOR, TLR, and MAPK signaling pathways. In the bar chart, the horizontal axis represents the value and the vertical axis represents the corresponding pathway name. The intensity of the color indicates a high degree of enrichment.

Interaction of nine core targets with active ingredients verified by molecular docking

To further validate the network pharmacology results, molecular docking was used to evaluate the identified active drug ingredients and targets. Nine core targets closely associated with AG (STAT3, SRC, MMP9, HIF1A, PPARG, TLR4, JUN, PTGS2 and NOS2) were selected as receptors; eight compounds, including higenamine, β-sitosterol, michelenolide, sinomenine, magnograndiolide, stepholidine, 16-epi-Isositsirikine and magnoflorine, were used as ligands for molecular docking; and the binding energies between the ligands and receptors were determined (Figure 3A). When the molecular docking binding energy is < 0, the two molecules have the ability to spontaneously bind; when the molecular docking binding energy is < -1.2 kcal/mol (-5.0 kJ/mol), the two molecules stably bind to each other[28].

The active components of *C. sinomenii* obtained from screening all bound to the selected targets. Inflammation plays an important role in gout development. Sinomenine alleviates inflammation by inhibiting the expression of the LPS receptor (CD14)/TLR4 and then activating the downstream Janus tyrosine kinase (JAK2)/STAT3 signaling pathway[36]. Sinomenine also treats rheumatoid arthritis by inhibiting the overexpression of the MMP9 protein[37]; inhibits the release of inflammatory factors by downregulating the expression of TLR4[38]; exerts anti-inflammatory and analgesic effects by regulating the expression of cyclooxygenase-2 (COX-2) and inhibiting the secretion of inflammatory factors[39]; and relieves pain and inflammation by inhibiting the expression of NOS2 and the production of nitric oxide (NO)[40]. β-sitosterol significantly inhibits the upregulation of TLR4 expression and alleviates inflammation[41]. Stepholidine alleviates gouty arthritis and inflammation by inhibiting TLR4 and NOS2 expression[42]. Therefore, the above eight compounds were selected for MD simulations (Figure 3B-I).

C. sinomenii exerted therapeutic effects by modulating TLR4 and PTGS2

The binding mode, stability, and molecular interactions of sinomenine with TLR4 and PTGS2 were investigated using MD simulations.

The root mean square deviation (RMSD) represents the sum of the deviations of all the atoms between the conformation at a certain time and the target conformation, and is an important basis for measuring the stability of the system. Variation in the RMSD of all atoms in the protein was demonstrated in the composite system versus time. The RMSD value of the protein molecules in the entire system fluctuated greatly at the beginning of the simulation, which might be due to the interaction between the protein and the solvent molecules at the beginning of the simulation. Subsequently, the overall RMSD stabilized. The average RMSD of the sinomenine-PTGS2 composite system was 7.082 ± 0.879 nm after stabilization, and the average RMSD of the sinomenine-TLR4 composite system was 2.974 ± 0.488 nm after stabilization. The small fluctuation amplitude indicated that the entire system was stable and reliable during the simulation (Figure 4A).

The radius of gyration (Rg) may be used to measure the compactness of the overall protein structure. If the folding of a protein is stable, then its Rg value remains relatively stable. A greater change in Rg indicates a greater change in the protein structure. The Rg values of the sinomenine-PTGS2 and sinomenine-TLR4 systems fluctuated slightly throughout the simulation; however, the fluctuations were relatively small. The average Rg values for the sinomenine-PTGS2 and sinomenine-TLR4 systems during the entire simulation process were 25.583 ± 0.363 nm and 56.502 ± 0.161 nm, respectively, indicating that the entire structure of the protein small-molecule complex was very stable during the simulation (Figure 4B).

The root mean square fluctuation (RMSF) represents the flexibility of protein amino acid residues. The RMSF values of all amino acids in the sinomenine-PTGS2 and sinomenine-TLR4 systems are shown in Figure 4. The overall RMSF value of the protein in the sinomenine-PTGS2 complex was small, and the RMSF values of the protein near position 360 and the N-terminal- and C-terminal domains significantly fluctuated. Solvent molecules had a significant effect. In addition, the overall RMSF value of the protein in the sinomenine-TLR4 complex fluctuated somewhat, indicating that these amino acids had high flexibility and might be located in the nonguided coil or turn region of the protein, or might protrude from the protein surface and be exposed to solvents. The RMSF results revealed that the protein structure combined with small molecules was relatively stable throughout the entire simulation process, which was conducive to the stable binding of small-molecule compounds and the corresponding biological functions (Figure 4C and D).

The variation in the number of hydrogen bonds between small molecules and proteins in a complex system as a function of simulation time was analyzed (Figure 4E and F). The average number of hydrogen bonds of small protein molecules in the sinomenine-PTGS2 composite system during the entire simulation process was 1.348 whereas the number of hydrogen bonds of small protein molecules in the sinomenine-TLR4 composite system was 1.348 during the whole simulation process. The mean value was 1.066. Stable hydrogen bonding between small molecules and proteins indicated that stable interactions occurred between these molecules and proteins during the entire simulation process, and that they performed their corresponding biological functions.

Next, the binding free energies were calculated between the protein and small molecules in the range of 80–100 ns, where the RMSD was more stable in the system, using the Molecular Mechanics/Poisson-Boltzmann Surface Area method. For the small molecules in the sinomenine-PTGS2 and sinomenine-

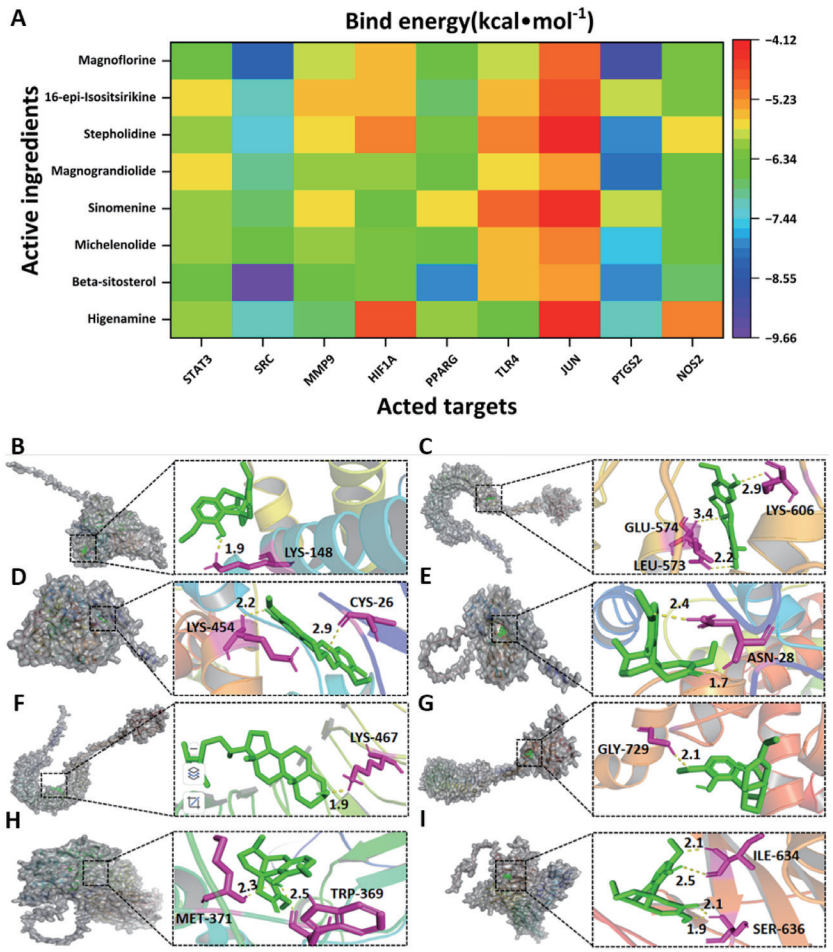

Fig. 3. **Molecular docking of core targets and visualization.**
(A) Molecular docking fraction heatmap analysis. (B) Docking poses and interactions of sinomenine with matrix metalloproteinase 9 (MMP9). (C) Docking poses and interactions of stepholidine with Toll-like receptor 4 (TLR4). (D) Docking poses and interactions of stepholidine with prostaglandin endoperoxide synthase 2 (PTGS2). (E) Docking poses and interactions of sinomenine with PTGS2. (F) Docking poses and interactions of β-sitosterol with TLR4. (G) Docking poses and interactions of sinomenine with TLR4. (H) Docking poses and interactions of sinomenine with inducible nitric oxide synthase 2 (NOS2). (I) Docking poses and interactions of sinomenine with signal transducer and activator of transcription 3 (STAT3). Nonreceptor tyrosine kinase (SRC); hypoxia-inducible factor 1A (HIF1A); peroxisome proliferator activated receptor G (PPARG); transcription factor AP-1 (JUN).

TLR4 systems, the total binding free energies between the small molecules and the protein were -76.493 kJ/mol and -56.998 kJ/mol, respectively. The electrostatic interactions of the system, including the electrostatic interactions under vacuum conditions and the polar solvation energy ($\Delta G_{ele}+\Delta G_{PB}$), were 62.580 kJ/mol and 65.368 kJ/mol, respectively. The nonpolar interaction may be used as the hydrophobic interaction energy, including the van der Waals force effect and the nonpolar solvation free energy ($\Delta G_{vdw}+\Delta G_{np}$). The nonpolar interactions were -139.074 kJ/mol and -122.366 kJ/mol, respectively. These results indicated that hydrophobic interactions between small molecules and proteins were the main driving forces of binding (Table 1).

The active ingredients from C. sinomenii had low toxicity in the treatment of AG

The predicted results are shown in Table 2, in which magnograndiolide and 16-epi-Isositsirikine are class III compounds

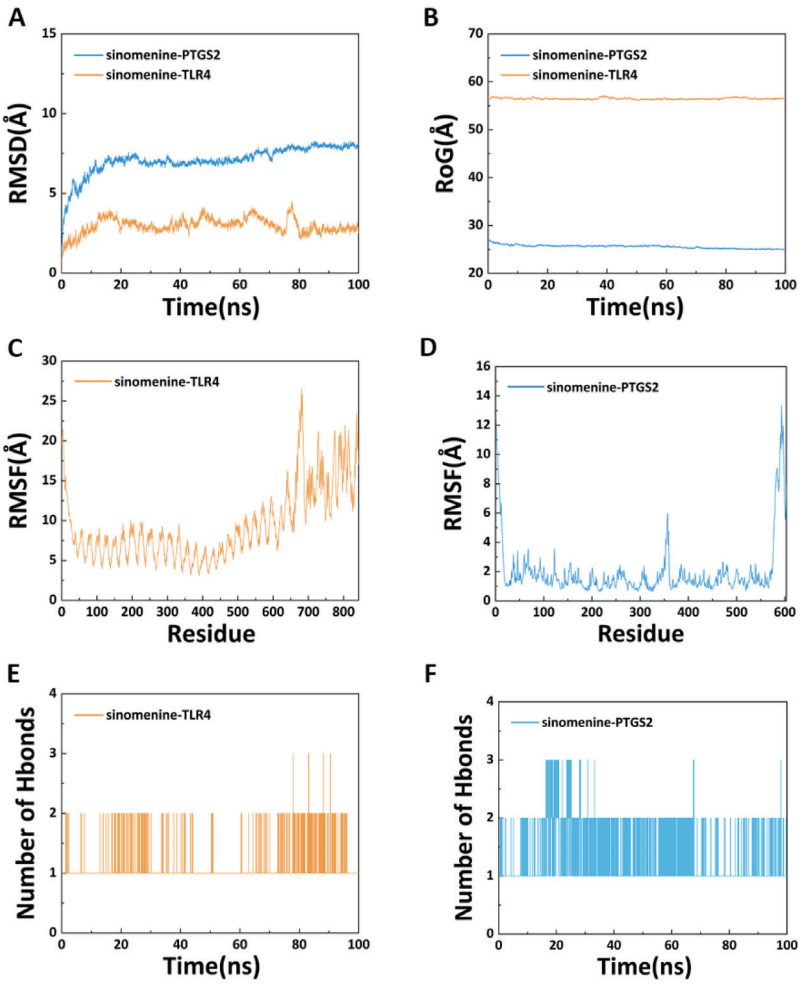

Fig. 4. **Molecular dynamics of Toll-like receptor 4 (TLR4) and prostaglandin endoperoxide synthase 2 (PTGS2) with residues in the active pocket of sinomenine.**

(A) The variation in the root mean square deviation (RMSD) values of protein molecules in the sinomenine-PTGS2 and sinomenine-TLR4 systems with simulation time. (B) The variation in the rotation radius of the sinomenine-PTGS2 and sinomenine-TLR4 systems with simulation time. (C) Root mean square fluctuation (RMSF) values of all amino acid residues in the sinomenine-TLR4 system. (D) RMSF values of all amino acid residues in the sinomenine-PTGS2 system. (E) Changes in the number of hydrogen bonds between proteins and small molecules in the sinomenine-TLR4 system over the simulation time. (F) Changes in the number of hydrogen bonds between proteins and small molecules in the sinomenine-PTGS2 system over the simulation time.

with toxic effects, β-sitosterol sinomenine, stepholidine, and magnoflorine are class IV compounds with harmful effects, and michelenolide is a class V compound with possible harmful effects. According to records in the Compendium of Materia Medica and the clinical trial protocol for human gout, the therapeutic dose of *C. sinomenii* was approximately 0.6 mg/kg body weight, which was significantly lower than the harmful dose.

Discussion

This study used network pharmacology to investigate the mechanism by which *C. sinomenii* treats AG by identifying the active components and targets of *C. sinomenii* and the re-

Table 1. **Binding free energy between small molecules and proteins.**

System	sinomenine-PTGS2		sinomenine-TLR4	
Item	Energy (kJ/mol)	Delta	Energy (kJ/mol)	Delta
ΔG_{vdw} (kJ/mol)	-124.411	9.662	-98.735	5.118
ΔG_{ele} (kJ/mol)	-18.384	0.672	-14.664	3.798
ΔG_{PB} (kJ/mol)	80.964	3.518	80.032	6.476
ΔG_{np} (kJ/mol)	-14.663	0.924	-23.631	2.744
ΔG_{bind} (kJ/mol)	**-76.493**	**4.641**	**-56.998**	**4.694**

ΔG_{vdw}: van der Waals force effect; ΔG_{ele}: electrostatic interactions; ΔG_{PB}: polar solvation energy; ΔG_{np}: nonpolar solvation free energy; ΔG_{bind}: binding free energy.

Table 2. **Molecular toxicity prediction of eight active ingredients from *C. sinomenii*.**

Active ingredient	Predicted Toxicity Class	Predicted LD50 (mg/kg)	Organ toxicity	Toxicity end points
Higenamine	V	3350	Respiratory toxicity	BBB-barrier Clinical toxicity
Beta-sitosterol	IV	890	Neurotoxicity Respiratory toxicity	Immunotoxicity BBB-barrier Ecotoxicity Nutritional toxicity
Michelenolide	V	2550	Respiratory toxicity	Immunotoxicity BBB-barrier Nutritional toxicity
Sinomenine	IV	580	Respiratory toxicity	Immunotoxicity BBB-barrier Clinical toxicity
Magnograndiolide	III	150	Respiratory toxicity	Immunotoxicity BBB-barrier Clinical toxicity Nutritional toxicity
Stepholidine	IV	928	Neurotoxicity Respiratory toxicity	Immunotoxicity BBB-barrier Clinical toxicity
16-epi-Isositsirikine	III	300	Neurotoxicity Nephrotoxicity Respiratory toxicity	BBB-barrier Clinical toxicity
Magnoflorine	IV	401	Respiratory toxicity	Immunotoxicity BBB-barrier

lated signaling pathways. Eight active components including alkaloids, sterols, and terpenes were identified. The drug-active ingredient-potential target-disease network diagram revealed that active ingredients, such as sinomenine, β-sitosterol, and stepholidine might play key roles in the treatment of AG with *C. sinomenii*. Sinomenine is an alkaloid monomer extracted from *C. sinomenii* that exerts pharmacological effects, such as anti-inflammatory and analgesic effects, by regulating the NOD-like receptor protein 3 (NLRP3) inflammasome signaling pathway, affecting the secretion of the inflammatory cytokine interleukin-1β (IL-1β) and IL-6, and thereby reducing the incidence of gouty arthritis[43,44]. β-sitosterol reduces serum uric acid levels in hyperuricemic mice by inhibiting xanthine oxidase (XOD) activity in the liver and by effectively inhibiting monosodium urate (MSU)-induced edema[45]. In addition, stepholidine alleviates gouty arthritis by inhibiting the expression of TLR4 and members of the NLRP3 inflammasome, and inhibiting NF-κB activation, lipid peroxidation, NO production, and COX-2 expression, thereby suppressing the inflammatory response[42]. Therefore, sinomenine, β-sitosterol, and stepholidine might be the main active ingredients in *C. sinomenii* for the prevention and treatment of AG.

In this study, multiple potential targets closely related to AG, including TLR4, MMP9, PTGS2, STAT3, and NOS2, which may play regulatory roles in the prevention and treatment of AG by *C. sinomenii* were identified by constructing a PPI network[46]. TLR4 may be involved in the regulation of gout-related inflammation by directly binding to MSU and increasing the production of inflammatory factors, such as NLRP3 and IL-1β[47]. TLR4 expression plays a key role in gouty arthritis[48]. Hyperuricemia

promotes the expression of MMP9 in synovial fluid and is associated with inflammation and gouty arthritis[49]. In gouty arthritis, sinomenine exerts its anti-inflammatory effects mainly by reducing the secretion of interleukins and MMP9 produced by monocytes in peripheral blood[50]. PTGS2 is significantly upregulated in gout and is involved in the synthesis of prostaglandins, promotion of inflammation, and pain sensation[51]. STAT3 reduces serum uric acid levels and alleviates renal fibrosis and chronic kidney disease[52]. Berberine in *Phellodendron amurense* inhibits the activation of the JAK/STAT3 signaling pathway to reduce the activity of XOD, and upregulate the mRNA and protein expression of organic anion transporter 1/organic anion transporter 3 and adenosine triphosphate binding cassette transporter G2 to reduce serum uric acid levels[53]. In addition, in gouty arthritis, MSU stimulates inflammatory cells to produce NOS2, which ultimately damages the joints[54]. Moreover, NOS2 induces inflammatory cells to produce proinflammatory cytokines, exacerbating inflammation[54]. These targets have been implicated in the pathogenesis of inflammation via various mechanisms, indicating that *C. sinomenii* may exert its efficacy against AG by acting on multiple targets, thus mitigating the inflammatory response.

KEGG pathway analysis revealed that the active ingredients of *C. sinomenii* mainly regulate the MAPK, mTOR, NOD-like receptor, and TLR signaling pathways. Uric acid disrupts the balance between pro- and anti-apoptotic proteins by regulating the MAPK pathway, leading to apoptosis[55]. This triggers oxidative stress in kidney cells, resulting in inflammation. Therefore, genes involved in positive regulation of the MAPK pathway may play a role in lowering uric acid levels. mTOR belongs to the PI3K protein kinase class and is a serine/threonine kinase involved in the regulation of cell growth, proliferation, and other processes. MSU activates autophagy and triggers cell death by inhibiting the activation of the mTOR signaling pathway[56,57]. The inflammasome is composed of a Nod-like receptor, such as NLRP1, NLRP3, or NLRP4, and an adapter apoptosis-associated speck-like protein containing a caspase recruitment domain. MSU is a danger signal formed after the release of uric acid by dead cells. It triggers cellular inflammation by activating the NLRP3 inflammasome, leading to the production of the active inflammatory cytokines IL-1β and IL-18[58]. TLRs are pattern recognition receptors present in the cell membrane and cytoplasm. The development of gouty arthritis is closely related to the ability of precipitated sodium urate to react with macrophages, leading to neutrophil aggregation and entry into the synovial and joint fluid. Neutrophils phagocytose sodium urate crystals in the synovial and joint fluid, a process in which lysosomes and cell membranes dissolve and leukocyte aggregation and inflammatory mediators are released. The release of inflammatory mediators further activates the TLR2/TLR4-NF-κB signaling pathway, creating a positive feedback loop that exacerbates inflammation[59]. These targets and pathways potentially increase the infiltration and activation of inflammatory cells, thereby exacerbating the inflammatory response. Conversely, *C. sinomenii* may exert anti-inflammatory effects against AG by modulating targeted signaling pathways.

According to the Compendium of Materia Medica, *C. sinomenii* is effective in treating arthritis, numbness, itching, and swelling. ZhengQingFengTongNing (National Medical Products Administration Approval Number Z20010174 in China) is a first-line medication, in which the active ingredient is an extract of *C. sinomenii*. An important advantage of this drug is that it is less likely to cause resistance, and its disadvantage is its short half-life (approximately 2–4 h), which makes it easy to metabolize and eliminate from the body. Extending the half-life and efficacy time is a bottleneck that must be overcome. However, this defect has become an advantage in veterinary clinical use, making it less likely to cause drug resistance and residues without toxicological risks in chickens or eggs. ZhengQingFengTongNing tablets contain 20 mg/tablet of sinomenine at a price of 50 yuan/bottle (100 tablets/bottle), which is approximately 0.5 yuan/tablet. The dosage for a 100 kg adult is 3 tablets, which is equivalent to a dosage of 0.6 mg/kg body weight. In poultry science, with laying hens as an example, the two high-frequency periods of AG are at 1 and 3 months. At this time, the weights of the hens were approximately 0.2 kg or 1 kg, respectively. The drug cost for 100–200 hens was the same as that for an adult, which was 1.5 yuan for a single use. Moreover, poultry medicine does not need to be processed into ZhengQingFengTongNing tablets, and the raw material may be directly used. The raw material of *C. sinomenii* is approximately 30 yuan per kilogram, of which, sinomenine comprises 1%–2%; there is 10–20 g of sinomenine per kilogram of *C. sinomenii* raw material. The drug cost for 100–200 hens was approximately 0.5 yuan. This approach is inexpensive for clinical veterinary use in the poultry industry.

In summary, *C. sinomenii*, whose main active ingredients were sinomenine, β-sitosterol, and stepholidine, had potential therapeutic effects on AG by acting on the following core targets: TLR4, PPARG, MMP9, STAT3, and NOS2, all of which were closely related to the MAPK, mTOR, NOD-like receptor, and TLR signaling pathways. These signaling pathways play key roles in the prevention and treatment of AG by regulating the inflammatory response. Therefore, the mechanism by which C. *sinomenii* protects against AG involves the synergistic effects of multiple components, targets, and pathways.

Acknowledgements

We thank all the organizations and individuals who provided generous help with this study.

Author contributions

Funding details: This work was supported by grants from the Natural Science Foundation of Hunan Province (2021JJ30546 and 2021JJ30547), Fund Project of Hunan Education Department (20K099 and 21A0495), and Natural Sciences Foundation of China (81830041 and 81771617).

Data availability statement

The data supporting the findings of this study are available from the corresponding author upon reasonable request.

Conflicts of interest

The authors declare no conflict of interest.

References

[1] Xiang Y, Chen M, Sun M, Dong J, Zhang J, Huang Y, Zhai Q, Liao M and Li L. Isolation, identification, and epidemiological characteristics of goose astrovirus causing acute gout in Guangdong province, China. Poult Sci, **103**: 104143. 2024. https://doi.org/10.1016/j.psj.2024.104143, PMID:39128392

[2] Bulbule NR, Mandakhalikar KD, Kapgate SS, Deshmukh VV, Schat KA and Chawak MM. Role of chicken astrovirus as a causative agent of gout in commercial broilers in India. Avian Pathol, **42**: 464–473. 2013. https://doi.org/10.1080/03079457.2013.828194, PMID:24015918

[3] Hong F, Zheng A, Xu P, Wang J, Xue T, Dai S, Pan S, Guo Y, Xie X, Li L, Qiao X, Liu G and Zhai Y. High-protein diet induces hyperuricemia in a new animal model for studying human gout. Int J Mol Sci, **21**: 2147. 2020. https://doi.org/10.3390/ijms21062147, PMID:32245084

[4] Liu C, Sun M and Liao M. A review of emerging goose astrovirus causing gout. BioMed Res Int, **2022**:1635373. 2022. https://doi.org/10.1155/2022/1635373, PMID:36072471

[5] Li L, Sun M, Zhang Y and Liao M. A review of the emerging poultry visceral gout disease linked to avian astrovirus infection. Int J Mol Sci, **23**: 10429. 2022. https://doi.org/10.3390/ijms231810429, PMID:36142340

[6] Zhang F, Li Y, Jiang W, Yu X, Zhuang Q, Wang S, Yuan L, Wang K, Sun S and Liu H. Surveillance and genetic diversity analysis of avian astrovirus in China. PLoS One, **17**: e0264308. 2022. https://doi.org/10.1371/journal.pone.0264308, PMID:35226672

[7] Patel MK, Dave DJ, Rathod RC, Joshi BP and Ghodasara DJ. Study on ameliorative effect of febuxostat on gout induced model in broiler chicks. Indian J Vet Sci Biotechnol, **13**. 2017. https://doi.org/10.21887/ijvsbt.v13i01.8734

[8] Huang H, Ding R, Chen Z, Yi Z, Wang H, Lv Y and Bao E. Goose nephritic astrovirus infection increases autophagy, destroys intercellular junctions in renal tubular epithelial cells, and damages podocytes in the kidneys of infected goslings. Vet Microbiol, **263**: 109244. 2021. https://doi.org/10.1016/j.vetmic.2021.109244, PMID:34649010

[9] Cronstein BN and Sunkureddi P. Mechanistic aspects of inflammation and clinical management of inflammation in acute gouty arthritis. J Clin Rheumatol, **19**: 19–29. 2013. https://doi.org/10.1097/RHU.0b013e31827d8790, PMID:23319019

[10] Wideman RF Jr, Roush WB, Satnick JL, Glahn RP and Oldroyd NO. Methionine hydroxy analog (free acid) reduces avian kidney damage and urolithiasis induced by excess dietary calcium. J Nutr, **119**: 818–828. 1989. https://doi.org/10.1093/jn/119.5.818, PMID:2723831

[11] Hocking PM, Gentle MJ, Bernard R and Dunn LN. Evaluation of a protocol for determining the effectiveness of pretreatment with local analgesics for reducing experimentally induced articular pain in domestic fowl. Res Vet Sci, **63**: 263–267. 1997. https://doi.org/10.1016/S0034-5288(97)90031-X, PMID:9491454

[12] Sherman MR, Saifer MGP and Perez-Ruiz F. PEG-uricase in the management of treatment-resistant gout and hyperuricemia. Adv Drug Deliv Rev, **60**: 59–68. 2008. https://doi.org/10.1016/j.addr.2007.06.011, PMID:17826865

[13] Vikrama Chakravarthi P, Murugesan S, Arivuchelvan A, Sukumar K, Arulmozhi A and Jagadeeswaran A. Therapeutic antigout and antioxidant activity of *Piper betle* L. in gout-induced broilers. Br Poult Sci, **63**: 324–331. 2022. https://doi.org/10.1080/00071668.2021.1998365, PMID:34859728

[14] Zhao XX, Peng C, Zhang H and Qin LP. *Sinomenium acutum*: A review of chemistry, pharmacology, pharmacokinetics, and clinical use. Pharm Biol, **50**: 1053–1061. 2012. https://doi.org/10.3109/13880209.2012.656847, PMID:22775422

[15] Liu Y, Liu C, Tan T, Li S, Tang S and Chen X. Sinomenine sensitizes human gastric cancer cells to cisplatin through negative regulation of PI3K/AKT/Wnt signaling pathway. Anticancer Drugs, **30**: 983–990. 2019. https://doi.org/10.1097/CAD.0000000000000834, PMID:31609766

[16] Lyu HN, Zeng KW, Cao NK, Zhao MB, Jiang Y and Tu PF. Alkaloids from the stems and rhizomes of Sinomenium acutum from the Qinling Mountains, China. Phytochemistry, **156**: 241–249. 2018. https://doi.org/10.1016/j.phytochem.2018.09.009, PMID:30340118

[17] Ru J, Li P, Wang J, Zhou W, Li B, Huang C, Li P, Guo Z, Tao W, Yang Y, Xu X, Li Y, Wang Y and Yang L. TCMSP: a database of systems pharmacology for drug discovery from herbal medicines. J Cheminform, **6**: 13. 2014. https://doi.org/10.1186/1758-2946-6-13, PMID:24735618

[18] Xu X, Bi J, Ping L, Li P and Li F. A network pharmacology approach to determine the synergetic mechanisms of herb couple for treating rheumatic arthritis. Drug Des Devel Ther, **12**: 967–979. 2018. https://doi.org/10.2147/DDDT.S161904, PMID:29731604

[19] Duan W, Chen J, Wu Y, Zhang Y and Xu Y. Protective effect of higenamine ameliorates collagen-induced arthritis through heme oxygenase-1 and PI3K/Akt/Nrf-2 signaling pathways. Exp Ther Med, **12**: 3107–3112. 2016. https://doi.org/10.3892/etm.2016.3730, PMID:27882125

[20] Cai Z, Feng Y, Li C, Yang K, Sun T, Xu L, Chen Y, Yan CH, Lu WW and Chiu KY. Magnoflorine with hyaluronic acid gel promotes subchondral bone regeneration and attenuates cartilage degeneration in early osteoarthritis. Bone, **116**: 266–278. 2018. https://doi.org/10.1016/j.bone.2018.08.015, PMID:30149068

[21] Haque MA, Jantan I, Harikrishnan H and Abdul Wahab SM. Magnoflorine enhances LPS-activated pro-inflammatory responses via MyD88-dependent pathways in U937 macrophages. Planta Med, **84**: 1255–1264. 2018. https://doi.org/10.1055/a-0637-9936, PMID:29906814

[22] Yang S, Chu S, Ai Q, Zhang Z, Gao Y, Lin M, Liu Y, Hu Y, Li X, Peng Y, Pan Y, He Q and Chen N. Anti-inflammatory effects of higenamine (Hig) on LPS-activated mouse microglia (BV2) through NF-κB and Nrf2/HO-1 signaling pathways. Int Immunopharmacol, **85**: 106629. 2020. https://doi.org/10.1016/j.intimp.2020.106629, PMID:32535536

[23] Luo W, Deng J, He J, Yin L, You R, Zhang L, Shen J, Han

Z, Xie F, He J and Guan Y. Integration of molecular docking, molecular dynamics and network pharmacology to explore the multi-target pharmacology of fenugreek against diabetes. J Cell Mol Med, **27**: 1959–1974. 2023. https://doi.org/10.1111/jcmm.17787, PMID:37257051

[24] Stelzer G, Rosen N, Plaschkes I, Zimmerman S, Twik M, Fishilevich S, Stein TI, Nudel R, Lieder I, Mazor Y, Kaplan S, Dahary D, Warshawsky D, Guan-Golan Y, Kohn A, Rappaport N, Safran M and Lancet D. The GeneCards suite: From gene data mining to disease genome sequence analyses. Curr Protoc Bioinformatics, **54**: 1.30.1-1.30.33. 2016. https://doi.org/10.1002/cpbi.5, PMID:27322403

[25] Zhou Y, Zhang Y, Zhao D, Yu X, Shen X, Zhou Y, Wang S, Qiu Y, Chen Y and Zhu F. TTD: *therapeutic Target Database* describing target druggability information. Nucleic Acids Res, **52**: D1465–D1477. 2024. https://doi.org/10.1093/nar/gkad751, PMID:37713619

[26] Li Q, Liu P, Wu C, Bai L, Zhang Z, Bao Z, Zou M, Ren Z, Yuan L, Liao M, Lan Z, Yin S and Chen L. Integrating network pharmacology and pharmacological validation to explore the effect of Shi Wei Ru Xiang powder on suppressing hyperuricemia. J Ethnopharmacol, **298**: 115679. 2022. https://doi.org/10.1016/j.jep.2022.115679, PMID:36058481

[27] Szklarczyk D, Gable AL, Nastou KC, Lyon D, Kirsch R, Pyysalo S, Doncheva NT, Legeay M, Fang T, Bork P, Jensen LJ and von Mering C. The STRING database in 2021: customizable protein–protein networks, and functional characterization of user-uploaded gene/measurement sets. Nucleic Acids Res, **49**: D605–D612. 2021. https://doi.org/10.1093/nar/gkaa1074, PMID:33237311

[28] Seeliger D and de Groot BL. Ligand docking and binding site analysis with PyMOL and Autodock/Vina. J Comput Aided Mol Des, **24**: 417–422. 2010. https://doi.org/10.1007/s10822-010-9352-6, PMID:20401516

[29] Van Der Spoel D, Lindahl E, Hess B, Groenhof G, Mark AE and Berendsen HJC. GROMACS: Fast, flexible, and free. J Comput Chem, **26**: 1701–1718. 2005. https://doi.org/10.1002/jcc.20291, PMID:16211538

[30] Jorgensen WL, Chandrasekhar J, Madura JD, Impey RW and Klein ML. Comparison of simple potential functions for simulating liquid water. J Chem Phys, **79**: 926–935. 1983. https://doi.org/10.1063/1.445869

[31] Darden T, York D and Pedersen L. Particle mesh Ewald: An $N\cdot\log(N)$ method for Ewald sums in large systems. J Chem Phys, **98**: 10089–10092. 1993. https://doi.org/10.1063/1.464397

[32] Hess B, Bekker H, Berendsen HJC and Fraaije JGEM. LINCS: A linear constraint solver for molecular simulations. J Comput Chem, **18**: 1463–1472. 1997. https://doi.org/10.1002/(SICI)1096-987X(199709)18:12<1463::AID-JCC4>3.0.CO;2-H

[33] Berendsen HJC, Postma JPM, van Gunsteren WF, DiNola A and Haak JR. Molecular dynamics with coupling to an external bath. J Chem Phys, **81**: 3684–3690. 1984. https://doi.org/10.1063/1.448118

[34] Martoňák R, Laio A and Parrinello M. Predicting crystal structures: the Parrinello-Rahman method revisited. Phys Rev Lett, **90**: 075503. 2003. https://doi.org/10.1103/PhysRevLett.90.075503, PMID:12633242

[35] Banerjee P, Kemmler E, Dunkel M and Preissner R. ProTox 3.0: a webserver for the prediction of toxicity of chemicals. Nucleic Acids Res, **52**: W513–W520. 2024. https://doi.org/10.1093/nar/gkae303, PMID:38647086

[36] Lai WD, Wang S, You WT, Chen SJ, Wen JJ, Yuan CR, Zheng MJ, Jin Y, Yu J and Wen CP. Sinomenine regulates immune cell subsets: potential neuro-immune intervene for precise treatment of chronic pain. Front Cell Dev Biol, **10**: 1041006. 2022. https://doi.org/10.3389/fcell.2022.1041006, PMID:36619869

[37] Luo J, Zhu Y, Yu Y, Chen Y, He K and Liu J. Sinomenine treats rheumatoid arthritis by inhibiting MMP9 and inflammatory cytokines expression: bioinformatics analysis and experimental validation. Sci Rep, **14**: 12786. 2024. https://doi.org/10.1038/s41598-024-61769-x, PMID:38834626

[38] Zhao Y, Li J, Yu K, Liu Y and Chen X. Sinomenine inhibits maturation of monocyte-derived dendritic cells through blocking activation of NF-kappa B. Int Immunopharmacol, **7**: 637–645. 2007. https://doi.org/10.1016/j.intimp.2007.01.007, PMID:17386411

[39] Wang X, Liu Y, Zhang H, Jin J, Ma Y and Leng Y. Sinomenine alleviates dorsal root ganglia inflammation to inhibit neuropathic pain via the p38 MAPK/CREB signalling pathway. Eur J Pharmacol, **897**: 173945. 2021. https://doi.org/10.1016/j.ejphar.2021.173945, PMID:33596416

[40] Gao WJ, Liu JX, Xie Y, Luo P, Liu ZQ, Liu L and Zhou H. Suppression of macrophage migration by down-regulating Src/FAK/P130Cas activation contributed to the anti-inflammatory activity of sinomenine. Pharmacol Res, **167**: 105513. 2021. https://doi.org/10.1016/j.phrs.2021.105513, PMID:33617975

[41] Zheng Y, Zhao J, Chang S, Zhuang Z, Waimei S, Li X, Chen Z, Jing B, Zhang D and Zhao G. β-Sitosterol alleviates neuropathic pain by affect microglia polarization through inhibiting TLR4/NF-κB signaling pathway. J Neuroimmune Pharmacol, **18**: 690–703. 2023. https://doi.org/10.1007/s11481-023-10091-w, PMID:38041701

[42] Kudo K, Hagiwara S, Hasegawa A, Kusaka J, Koga H and Noguchi T. Cepharanthine exerts anti-inflammatory effects via NF-κB inhibition in a LPS-induced rat model of systemic inflammation. J Surg Res, **171**: 199–204. 2011. https://doi.org/10.1016/j.jss.2010.01.007, PMID:20334881

[43] Dong HC, Li PN, Chen CJ, Xu X, Zhang H, Liu G, Zheng LJ and Li P. Sinomenine attenuates cartilage degeneration by regulating miR-223-3p/NLRP3 inflammasome signaling. Inflammation, **42**: 1265–1275. 2019. https://doi.org/10.1007/s10753-019-00986-3, PMID:30847744

[44] Li J, Deng H, Yao Y, Wang W, Hu J, Dong Y, Wang P, Liu L, Liu Z, Xie Y, Lu L and Zhou H. Sinomenine ameliorates collagen-induced arthritis in mice by targeting GBP5 and regulating the P2X7 receptor to suppress NLRP3-related signaling pathways. Acta Pharmacol Sin, **44**: 2504–2524. 2023. https://doi.org/10.1038/s41401-023-01124-4, PMID:37482570

[45] Ferraz-Filha Z, Michel Araújo M, Ferrari F, Dutra I and Saúde-Guimarães D. *Tabebuia roseoalba: In vivo* hypouricemic and anti-inflammatory effects of its ethanolic extract and constituents. Planta Med, **82**: 1395–1402. 2016. https://doi.org/10.1055/s-0042-105878, PMID:27159671

[46] Qing YF, Zhou JG, Zhang QB, Wang DS, Li M, Yang QB, Huang CP, Yin L, Pan SY, Xie WG, Zhang MY, Pu MJ and Zeng M. Association of TLR4 Gene rs2149356 polymorphism with primary gouty arthritis in a case-control study.

PLoS One, **8**: e64845. 2013. https://doi.org/10.1371/journal.pone.0064845, PMID:23738004

[47] Park BS and Lee JO. Recognition of lipopolysaccharide pattern by TLR4 complexes. Exp Mol Med, **45**: e66. 2013. https://doi.org/10.1038/emm.2013.97, PMID:24310172

[48] Liu L, He S, Jia L, Yao H, Zhou D, Guo X and Miao L. Correlation analysis of serum TLR4 protein levels and TLR4 gene polymorphisms in gouty arthritis patients. PLoS One, **19**: e0300582. 2024. https://doi.org/10.1371/journal.pone.0300582, PMID:38652726

[49] Hsieh MS, Ho HC, Chou DT, Pan S, Liang YC, Hsieh TY, Lan JL and Tsai SH. Expression of matrix metalloproteinase-9 (gelatinase B) in gouty arthritis and stimulation of MMP-9 by urate crystals in macrophages. J Cell Biochem, **89**: 791–799. 2003. https://doi.org/10.1002/jcb.10530, PMID:12858344

[50] Zeng M and Tong Q. Anti-inflammation effects of sinomenine on macrophages through suppressing activated TLR4/NF-κB signaling pathway. Curr Med Sci, **40**: 130–137. 2020. https://doi.org/10.1007/s11596-020-2156-6, PMID:32166675

[51] van Durme CMPG, Wechalekar MD, Landewé RBM, Pardo Pardo J, Cyril S, van der Heijde D and Buchbinder R. Non-steroidal anti-inflammatory drugs for acute gout. Cochrane Database Syst Rev, **2021**: CD010120. 2021. https://doi.org/10.1002/14651858.CD010120.pub3, PMID:34882311

[52] Pan J, Shi M, Guo F, Ma L and Fu P. Pharmacologic inhibiting STAT3 delays the progression of kidney fibrosis in hyperuricemia-induced chronic kidney disease. Life Sci, **285**: 119946. 2021. https://doi.org/10.1016/j.lfs.2021.119946, PMID:34516993

[53] Lin G, Yu Q, Xu L, Huang Z, Mai L, Jiang L, Su Z, Xie J, Li Y, Liu Y, Lin Z and Chen J. Berberrubine attenuates potassium oxonate- and hypoxanthine-induced hyperuricemia by regulating urate transporters and JAK2/STAT3 signaling pathway. Eur J Pharmacol, **912**: 174592. 2021. https://doi.org/10.1016/j.ejphar.2021.174592, PMID:34699754

[54] Peng YJ, Lee CH, Wang CC, Salter DM and Lee HS. Pycnogenol attenuates the inflammatory and nitrosative stress on joint inflammation induced by urate crystals. Free Radic Biol Med, **52**: 765–774. 2012. https://doi.org/10.1016/j.freeradbiomed.2011.12.003, PMID:22198264

[55] Jang MG, Song H, Kim JH, Oh JM, Park JY, Ko HC, Hur SP and Kim SJ. Prevention of hyperuricemia by *Clerodendrum trichotomum* leaf extract in potassium oxonate-induced mice. Dev Reprod, **24**: 89–100. 2020. https://doi.org/10.12717/DR.2020.24.2.89, PMID:32734126

[56] Xiao L, Lin S, Xu W and Sun E. Downregulation of Sox8 mediates monosodium urate crystal-induced autophagic impairment of cartilage in gout arthritis. Cell Death Discov, **9**: 95. 2023. https://doi.org/10.1038/s41420-023-01388-z, PMID:36918540

[57] Hwang H, Yang C, Park S and Kim H. Monosodium urate crystal-induced chondrocyte death via autophagic process. Int J Mol Sci, **16**: 29265–29277. 2015. https://doi.org/10.3390/ijms161226164, PMID:26670233

[58] Martinon F, Pétrilli V, Mayor A, Tardivel A and Tschopp J. Gout-associated uric acid crystals activate the NALP3 inflammasome. Nature, **440**: 237–241. 2006. https://doi.org/10.1038/nature04516, PMID:16407889

[59] Bodofsky S, Merriman TR, Thomas TJ and Schlesinger N. Advances in our understanding of gout as an auto-inflammatory disease. Semin Arthritis Rheum, **50**: 1089–1100. 2020. https://doi.org/10.1016/j.semarthrit.2020.06.015, PMID:32916560